A flower-like glomerophyric diorite porphyry from Central China: Constraints on the unusual texture

Yu-Xiang Zhu [a], Lian-Xun Wang [a,*], Chang-Qian Ma [a], Chao Zhang [b]

[a] State Key Laboratory of Geological Processes and Mineral Resources, School of Earth Sciences, China University of Geosciences, 430074 Wuhan, China
[b] Institut für Mineralogie, Leibniz Universität Hannover, Callinstr. 3, 30167 Hannover, Germany

ARTICLE INFO

ABSTRACT

An unusual texture with plagioclase phenocrysts clustered as flower-like glomerocrysts has been discovered in the Wulong diorite porphyry at the southern margin of North China Craton. The rock consists mainly of plagioclase and amphibole, with the former as dominant phenocryst. Two groups of the plagioclase phenocrysts have been distinguished: flower-like glomerocrysts (FG-type) and single isolated phenocrysts (SP-type). Chemical compositions of both FG- and SP-type plagioclases are similar in anorthite contents (An_{35-45}) which are slightly higher than the matrix (An_{25-35}). Calculation of the plagioclase crystallization time based on Crystal Size Distribution (CSD) program shows that the FG-type crystals have been formed within a longer timescale (226–2782 years) than the SP-type crystals (98–1910 years). The concave down CSDs and lack of small crystals for FG-type plagioclases suggest that coarsening may have been involved. In contrast, a concave-up CSD within the size of 3–10 mm plagioclase, indicating that a rejuvenation kinetic process after coarsening. A possible formation history for the unusual flower-like plagioclase glomerocrysts was proposed as follows. (1) Initial nucleation and growth of single crystals in a confined environment. (2) Ascent of early crystals with magma upwelling and radial coarsening at the roof layer of magma chamber. (3) Remobilization of dense crystal mush and final emplacement at shallow level of crust. (4) Rapid cooling and extensive nucleation and growth of matrix. (5) Postmagmatic alteration and metamorphism. It is likely that the morphologic diversity of plagioclase glomerocrysts is largely influenced by variation of undercooling degrees. The second step is the most important for the formation of the flower-like glomerophyric texture which requires an environments of relatively low undercooling degree.

1. Introduction

Glomerocryst texture refers to aggregation of a few to several monomineralic phenocrysts in igneous rocks, which is generally common in both volcanic and plutonic rocks. It has been previously reported to be morphologically and genetically diverse in volcanic or sub-volcanic rocks, for example, (1) the glomeroporphyritic aggregates from the DSDP Legs 45 and 46 at the mid-Atlantic ridge (Kuo and Kirkpatrick, 1982), the Timok Magmatic Complex in Eastern Serbia (Milovanović et al., 2005), the Chanho area in China (Xu et al., 2009), and the Okinawa Trough in Japan (Lai et al., 2016), (2) the radiating clusters from the Emeishan lava in southwest China (Cheng et al., 2014) and the Keweenawan flood basalts in Mamainse Point Area, Ontario (Annells, 1973; Giblin, 1974; Giblin and Armsburst, 1969), (3) the subparallel clusters in basalt from the Deccan traps in India (Higgins and Chandrasekharam, 2007; Ikeda et al., 2002; McBirney and Noyes, 1979), the Squire Greek Pluton in Washington and the

Barren Island in NE India ocean (Renjith, 2014; Vance, 1969), and (4) the cumulophyric aggregation in rhyolite from the Poe Mountain anorthosite in southeast Wyoming, the Oligocene rhyolite in Ethiopian Plateau and the volcanics in Central Eastern Sinai Egypt, Wadi Khliefiya (Barbey et al., 2005; Samuel et al., 2007; Scoates, 2000). In deep-level intrusive rocks, glomerophyric texture are relatively rare and mostly as cumulative aggregates, such as the Rocky Hill granodiorite in Tulare County, California (Putman and Alfors, 1969), the Cathedral Peak granodiorite in California, U.S.A (Higgins, 2017), the Northport granite in Maine, U.S.A. (Hogan, 1993), the mafic dykes from Eocene Big Timber Stock, south-central Montana (du Bray and Harlan, 1996), and the Skaergaard gabbroic and syenitic bodies in East Greenland (Holness et al., 2006). The most common glomerocryst is plagioclase (e.g. Cheng et al., 2014; Higgins, 2017; Higgins and Chandrasekharam, 2007; Lai et al., 2016; Milovanović et al., 2005; Renjith, 2014; Samuel et al., 2007; Seaman, 2000), but olivine (Schwindinger, 1999; Xu et al., 2009), pyroxene (Seaman, 2000; Xu et al., 2009) and quartz (Graeter et al., 2015; Vance, 1969) can also form glomerocrysts.

Several models have been proposed to interpret the glomerophyric texture: (1) synneusis model, in which sub-parallel crystals drifting

together to form the aggregation as a result of convective movement (e.g. Hogan, 1985; Kuo and Kirkpatrick, 1982; Schwindinger, 1999; Vance, 1969), (2) accumulation model, which formed by gravity setting in a pre-emplacement magma chamber (e.g. Higgins, 2005; Higgins and Chandrasekharam, 2007; Samuel et al., 2007; Scoates, 2000; Xu et al., 2009), (3) heterogeneous nucleation model, in which different crystals grow radiating along different directions (Cheng et al., 2014; McBirney and Noyes, 1979), (4) resorption model of large crystals (Hogan, 1993). Glomerocrysts are commonly distributed randomly without a preferred orientation. One simple model is likely not able to interpret the genesis of glomerocrysts in all cases, in which a series of crystallization kinetics and magma processes, e.g., convection, turbulence, degassing and magma mixing, etc., may have exerted combined effects (e.g. Higgins, 1998; Renjith, 2014; Shane, 2015; Weinberg et al., 2001). In recent years, the Crystal Size Distribution (CSD) theory, which was originated in chemical engineering (Randolph and Larson, 1971), has become a common approach used to constrain the residence time (or crystallization time) of phenocrysts (e.g. Cheng et al., 2014; Higgins and Chandrasekharam, 2007; Marsh, 1988). These quantitative studies can provide insight into physical processes and kinetics of magma and crystals, such as magma emplacement and multi-stage cooling (Cashman and Marsh, 1988; Cheng et al., 2017; Marsh, 1998; Simakin and Bindeman, 2008; Wang et al., 2014, 2015; Yang, 2012; Yang et al., 2014), textural coarsening (Higgins, 2009, 2011b; Magee et al., 2010), mineral growth, compaction and recrystallization (Cashman, 1993), as well as magma ascent rates and cooling history (Armienti et al., 2013).

In this paper, we focus on a recently discovered flower-like glomerophyric diorite porphyry dyke from Central China. With detailed studies on petrography, mineral chemistry and CSD calculations, we aim to shed new lights on the origin and formation of the unusual flower-like glomerophyric texture.

2. Geological setting and sample description

The Wulong glomerophyric diorite porphyry is located within the southern margin of the North China Craton (S-NCC) in central China (Fig. 1a). The S-NCC is a transition zone between the Qinling Orogenic belt and the North China Craton (NCC), bounded by the NNW-trending Sanmenxia-Lushan Fault (Fig. 1a). The oldest basement rocks of the S-NCC consist mainly of the Neoarchean-Paleoproterozoic Taihua Group (2.84–1.97 Ga), which is composed of a set of middle to high grade metamorphic rocks including TTG gneisses, amphibolites and marbles (Liu et al., 2009). It is locally uncomformably overlain by the Paleoproterozoic Tietonggou Formation in the Xiaoqinling area (1.91–1.80 Ga), which consists prominently of quartzites (Diwu et al., 2014). It is in turn covered by the extensively exposed Xiong'er Group, which is composed mainly of intermediate-acidic lavas and pyroclastic rocks. The Xiong'er Group is in turn uncomformably overlain by Meso-Neoproterozoic sedimentary rocks including the Guandaokou Group, the Ruyang Group and the Luanchuan Group. Neoarchean and Early Proterozoic intermediate-mafic magmatism and Mesozoic granitic magmatism are common in this region, but Paleozoic records are lacking.

The Wulong village is located in the south-southeast of Luoyang city in Henan province (34°30.98′ N, 112°40.43′ E) (Fig. 1a). The glomerophyric diorite porphyry outcrops behind the village. It is exposed as three small dykes (maximum width 20 m) intruded into the Archean migmatized biotite-plagioclase gneiss (Fig. 1b). The dykes are parallel to each other and NWW trending. The rocks show a typical porphyritic texture with plagioclase as the dominant phenocryst. In many cases, the plagioclase phenocrysts are clustered to form flower-like glomerocrysts (Fig. 2a, b), a special texture that has rarely been reported in literature (Annells, 1973; Giblin, 1974). For non-geologists, the glomerocrysts are well known as the "Luoyang peony stone", since the city of Luoyang is famous for peony flowers.

Based on different morphology, the plagioclase phenocrysts can be grouped into two main types: (1) Flower-like glomerocrysts (FG-type), in which small plagioclase crystals gathering in the center and larger crystals radially distributed in the outer part. Dark fine grained matrix (mainly amphibole and plagioclase) fills the residual space of the inner part. The glomerocrysts resemble the flowers. The size of glomerocrysts varies from 1 to 8 cm in diameter. The number of plagioclase crystals aggregated in an individual glomerocryst is generally about 10–15. Note that there are also few irregular-shaped glomerocryst with fewer aggregated plagioclase crystals sub-parallel to or touch each other (Fig. 2b, c). (2) Single isolated phenocrysts (SP-type), which have a variable particle size within 0.5 to 4.5 cm. In most cases, the SP-type phenocrysts are tabular (Fig. 2d) with a few in stumpy shape (Fig. 2e). Some large tabular crystals (~2 cm) appear to have irregular narrow hollows that are filled with fine-grained material
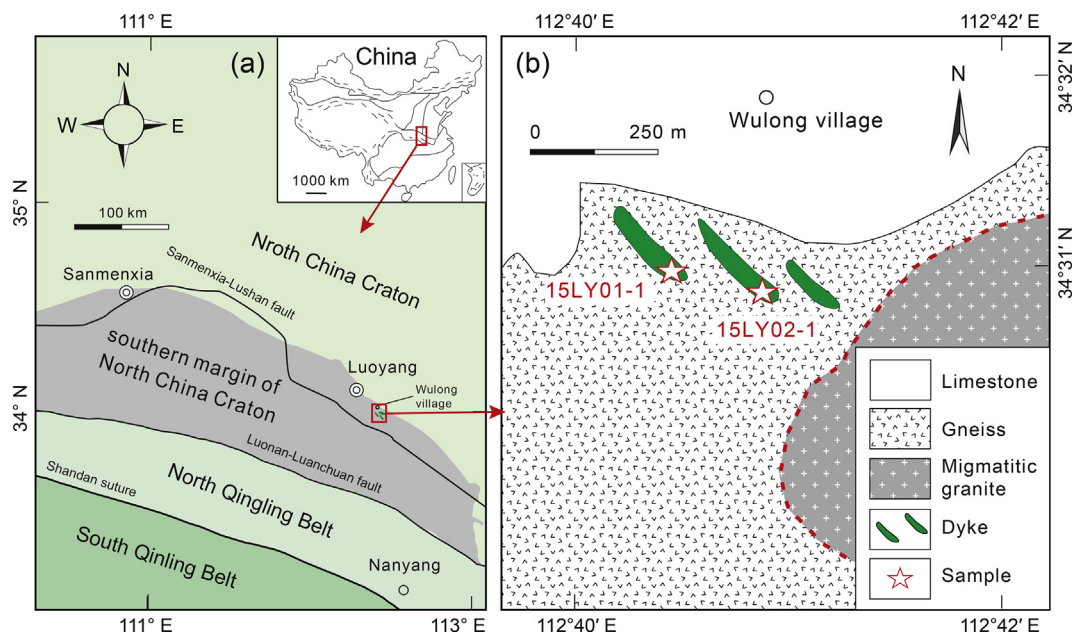
Fig. 1. (a) Geological sketch map of the Qinling Belt and the location of the study area (in frame) (modified after Dong and Santosh, 2016). (b) Simplified geological map of Wulong glomerophyric diorite porphyry dyke (after 1/200,000 geological map).
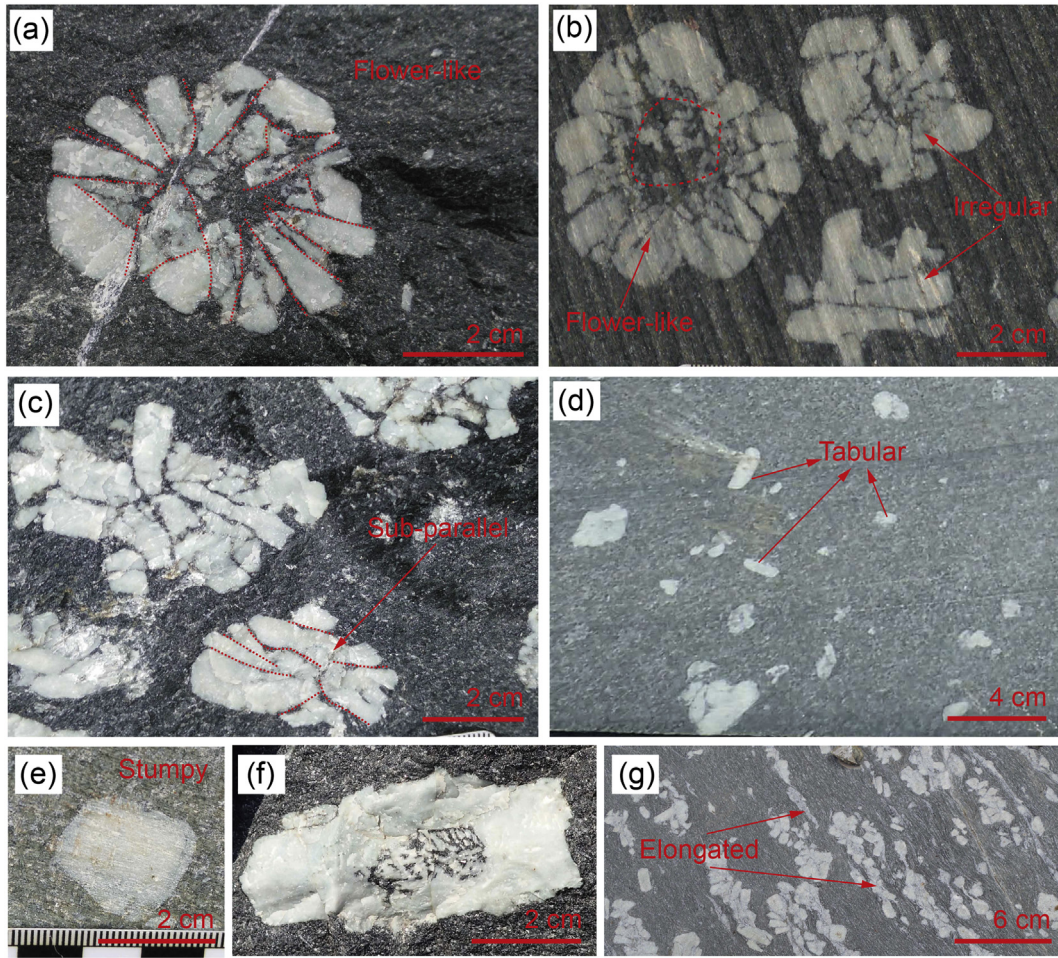
Fig. 2. Classification and textural characteristics of plagioclase phenocrysts: (a, b) Flower-like glomerocrysts, (b) Irregular-shaped glomerocrysts, (c) Sub-parallel glomerocrysts, (d) Single tabular phenocrysts, (e) Single massive phenocrysts, (f) Single tabular phenocrysts with irregular narrow hollows, (g) Elongated flower-like glomerocrysts and elongated lenticular single phenocrysts.
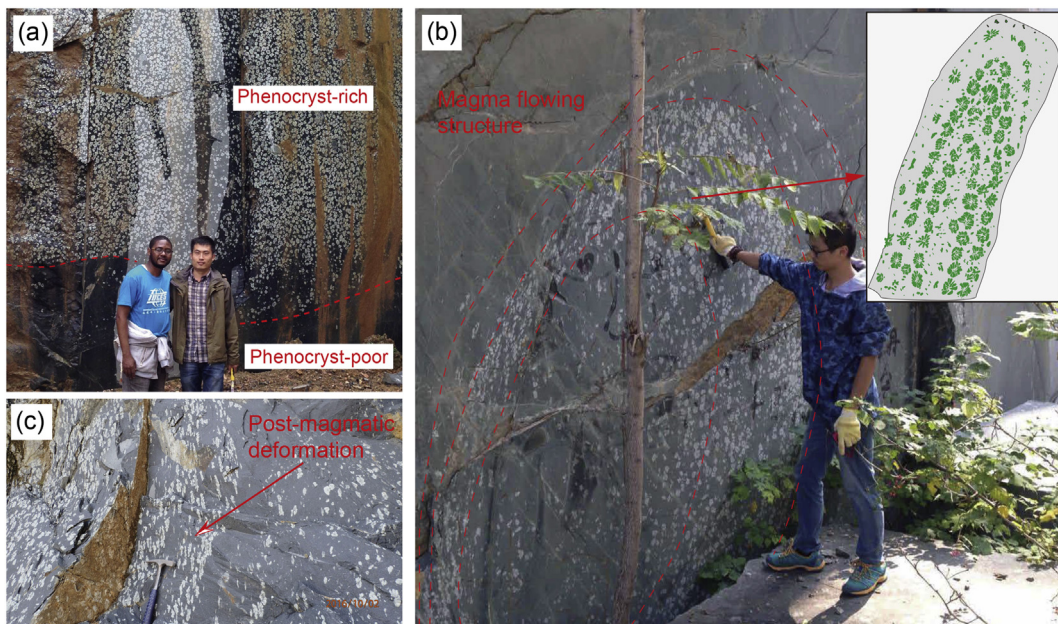
Fig. 3. Field photographs of the Wulong glomerophyric diorite porphyry. (a) Plagioclase phenocrysts are likely to enriched in the dyke center and reducing towards dyke margins. (b) Magma flowing structures presented in the dykes. (c) Elongated flower-like plagioclase glomerocrysts resulted from post-magmatic deformation.

similar to the matrix (Fig. 2f). Spatial distribution of plagioclase phenocrysts is unequal, commonly highly enriched in the dyke center and reducing towards the margins (Fig. 3a). A magma flowing structure is observed in one outcrop, with plagioclase phenocrysts showing preferred orientations (Fig. 3b).

The matrix mainly consists of plagioclase (50%) and amphibole (35%), minor biotite (5%) and quartz (5%) with accessory titanite, garnet, ilmenite and zircon. Plagioclase in the matrix is much smaller than the smallest phenocrysts, with length of 0.1 to 1 mm. They generally appear alone or locally aggregated, tending to distribute around the phenocrysts. It is also important to note that abundant secondary minerals formed via alteration and/or metamorphism are common in the rocks, resulting in almost all plagioclase phenocrysts, in particular in the center parts, altered to sericite and/or clinozoisite (Fig. 4a, b). Alteration degrees are highly dependent on grain size in plagioclase crystals. Fresh plagioclase rims with sericitized core is common for phenocryst (Fig. 4c),

whereas plagioclase matrix is almost fresh with typical albitic polysynthetic twin (Fig. 4d). Amphibole is anhedral, broken severely, and partially altered to chlorite (Fig. 4d, e), filling gaps in the matrix plagioclase.

A post-magmatic deformation structure has been observed in one outcrop of the Wulong diorite dyke with elongated plagioclase glomerocrysts or elongated lenticular plagioclase single phenocrysts (Fig. 2g). These elongated phenocrysts appear to be aligned and occur only in the rock fracture zone (Fig. 3c), indicating a strong internal deformation during solid state. Crystals of the matrix are also distorted and deformed to show a linear alignment, surrounding the aligned and/or imbricated phenocrysts (Fig. 2g). Very fine quartz and amphibole crystals form a strip or ring and are densely distributed in around the plagioclase phenocrysts and euhedral garnet (monocrystalline or twin, mainly almandine) occasionally inset the edge of the plagioclase phenocrysts, which indicates the influence of late-stage metamorphism on these rocks (Fig. 4f, g).
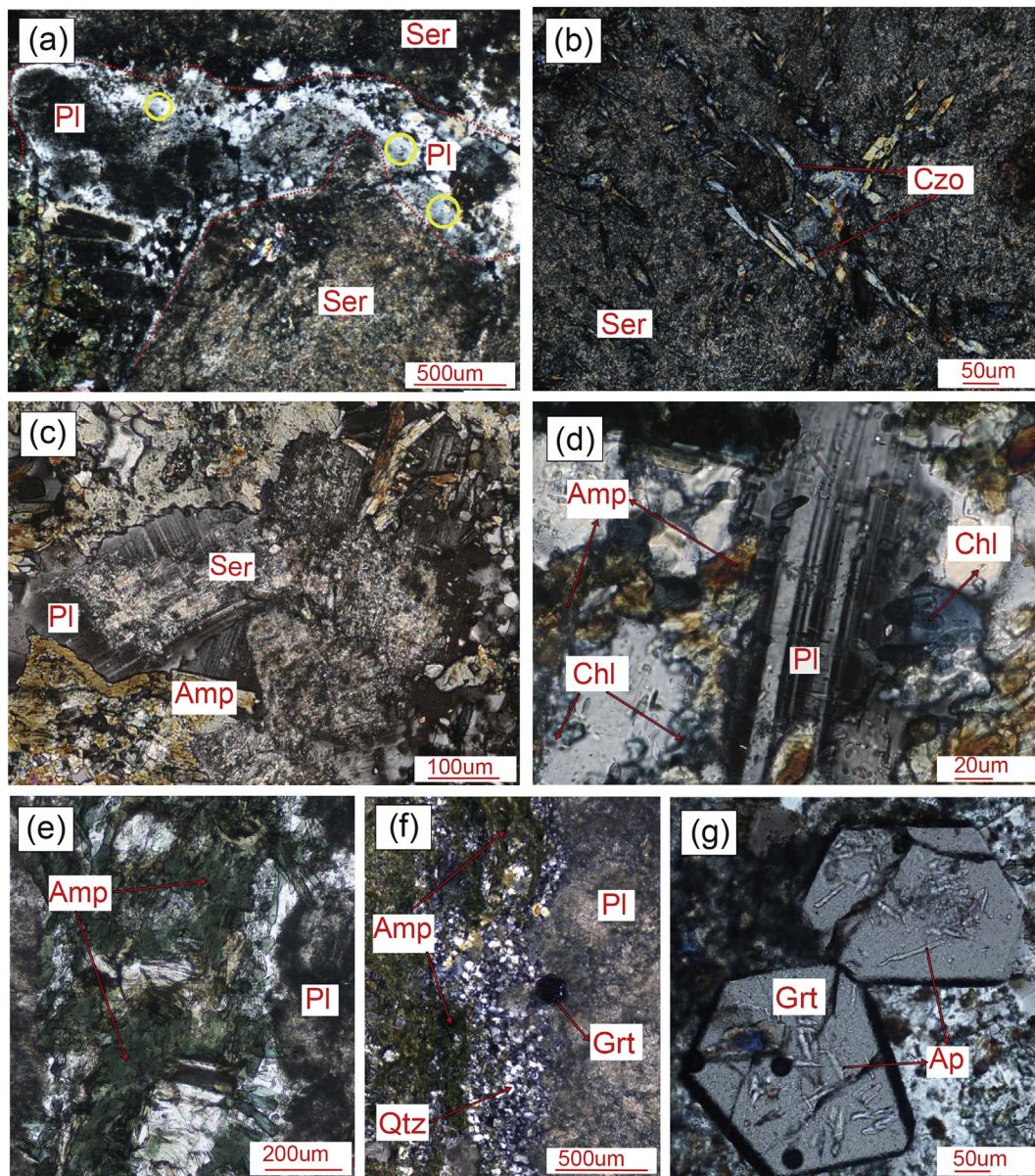
Fig. 4. Representing photomicrographs showing mineral assemblage and textural features of the Wulong glomerophyric diorite porphyry. (a, b) Large plagioclase phenocrysts are strongly altered to sericite and/or zoisite. (c) Fresh rims are preserved in smaller plagioclase phenocrysts. (d) Plagioclase matrix is mostly fresh with typical albitic polysynthetic twins. (e) Amphibole matrix is anhedral and partially altered to chlorite. (f) Quartz distributes densely on the rim of plagioclase phenocrysts. (g) Euhedral garnets occur in the plagioclase phenocrysts. Mineral abbreviations: *Ap* apatite, *Amp* amphibole, *Chl* chlorite, *Czo* clinozoisite, *Grt* garnet, *Pl* plagioclase, *Qtz*, quartz, *Ser* sericite.

3. Analytical methods

3.1. Mineral compositions

Mineral compositions were measured with electron microprobe analysis (EMPA) using a JEOL JXA 8230 Superprobe at the Center of Material Research and Analysis, Wuhan University of Technology, China. The quantitative analysis of plagioclase and garnet was performed with an acceleration voltage of 15 kV and a beam current of 10 nA. The electron beam spot was 10 um in diameter. The analytic accuracy is better than 1% for major elements (contents >5%) and 5% for minor elements (contents ~1%). X-ray compositional (Na, K) mapping was carried out on plagioclase glomerocryst using a Inca X-Act Energy Dispersive Spectrometer (EDS), with beam voltage of 15 kV, current of 10 nA and count time of 10–20 min per element for each image.

3.2. Crystal size distribution (CSD) measurement

Six representative samples (FG- and SP-type) for textural analysis have been conducted. High-resolution photographs of dissected longitudinal sections (0.8 m² to 1 m² area) were firstly taken in the field quarry. The selected photographs were subsequently scaled to facilitate the measurement of crystal size. The crystal margins are manually traced with a vector drafting program (CorelDraw). The plagioclase phenocrysts analyzed are over 3 mm long, taking into account of the photograph sharpness and data uncertainty. For touching crystals in the FG-type samples, the complete phenocrysts are identified by selecting the larger and more euhedral crystals, with a clear border. The other touching crystals with irregular shapes are depicted as an incomplete phenocryst. This procedure has been proven useful in reducing the resulted errors (Cheng et al., 2014). The crystal outlines are then filled and output as tiff files (Fig. 5). The ImageJ 1.42 software was used to analyze the binary grayscale and acquire two-dimensional parameters of crystals. The CSD of the plagioclase phenocrysts was then calculated with the program CSDCorrections 1.50 (Higgins, 2000, 2015).

The mean crystal shape is reflected by the crystal aspect ratio of short/intermediate/long axes (S/I/L), which is mainly estimated by the CSDSlice5 spreadsheet (Morgan and Jerram, 2006). Additional I/L ratio data are obtained from the measurements on the outcrops and the mode of the distribution of intersection width/intersection lengths (Higgins, 1994). Detailed theoretical introduction and analytical procedure can be found in Higgins (2006). Roundness is estimated to be 0.5 to 0.6 based on visual observations (0 = block, 1 = ellipsoid; Table 1). The alignment factor (AF) is calculated with the 40 largest crystals (100 = absolutely oriented, 0 = randomly distributed; Williams et al., 2006).
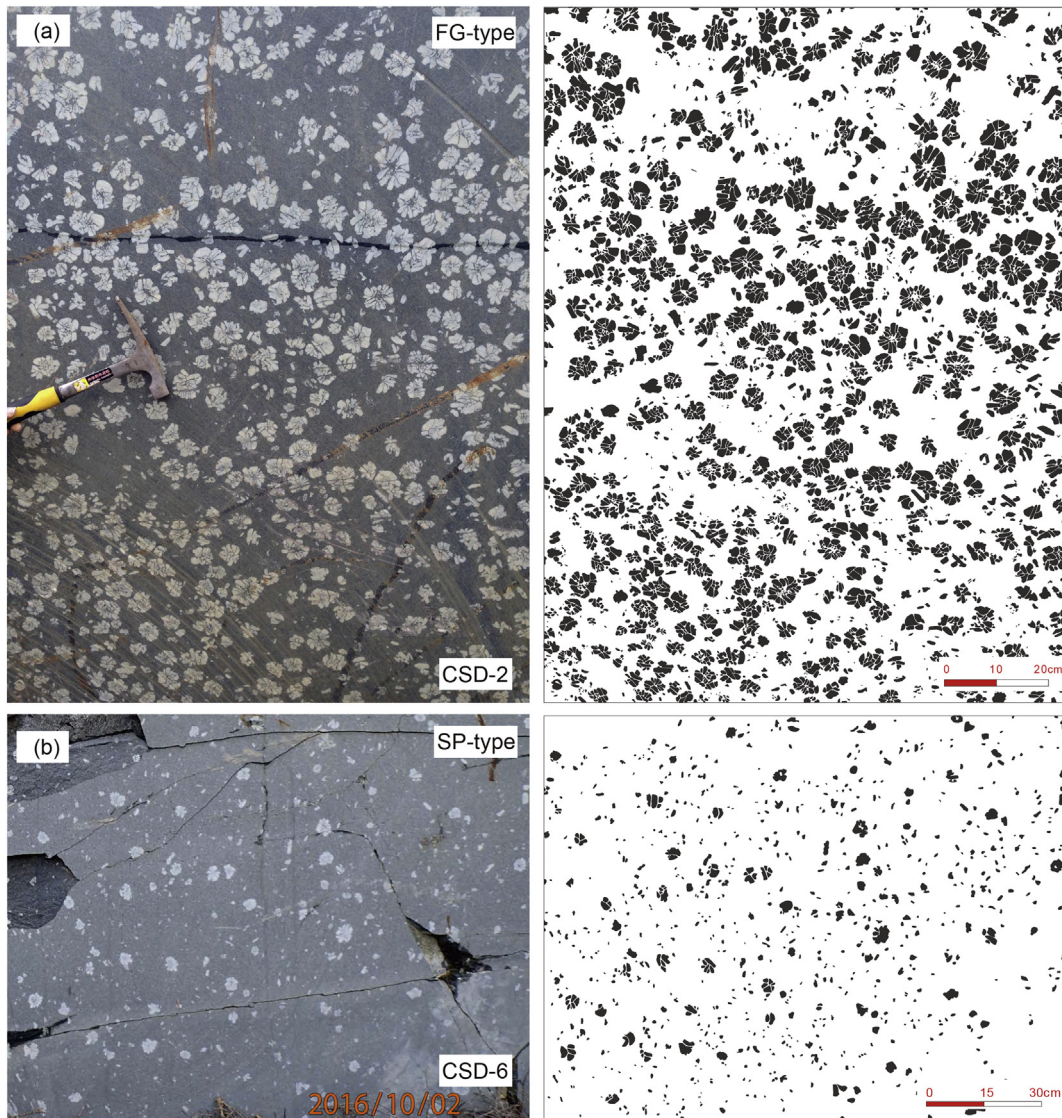
Fig. 5. Typical field photographs and outline images of FG-type and SP-type plagioclase phenocrysts. (a) FG-type sample CSD-2. (b) SP-type sample CSD-6.

Table 1
Textural parameters of the Wulong glomerophyric diorite porphyry samples.

Samples	Type	AR	Roundness	AF	I/S	L/I	No.	Area (cm²)	Vol phase (%)	CSD volume (%)	Regression volume (%)	Intercept	Error (1δ)	CSD slope	Error (1δ)	CSD CL/cm	LS Slope	LS CL/cm	Crystallization time (year)
CSD-1-1	FG-type	1:2.3:2.3	0.5	19	2.3	1.4	1942	13,305	20.17	20.20	25.52	-1.51	0.06	-1.14	0.03	0.88	-1.15	0.87	278–2782
CSD-2-1	FG-type	1:2.3:2.3	0.5	5	2.2	1.0	284,747	13,635	22.46	22.60	28.46	-0.89	0.05	-1.30	0.03	0.77	-1.42	0.70	244–2439
CSD-3-1	FG-type	1:2.3:2.3	0.6	34	1.8	1.5	416	8687	4.64	4.64	6.19	-2.29	0.13	-1.34	0.07	0.71	-1.31	0.76	226–2265
CSD-1-2	SP-type	1:2.3:2.3	0.5	19	2.0	1.4	465	13,305	2.66	2.66	2.61	-2.06	0.10	-1.76	0.06	0.57	-1.40	0.71	180–1802
CSD-2-2	SP-type	1:2.3:2.3	0.6	11	2.0	1.1	989	13,635	4.27	4.26	4.27	-1.08	0.07	-1.96	0.05	0.51	-2.00	0.50	162–1618
CSD-3-2	SP-type	1:2.3:2.3	0.6	18	1.9	1.4	1067	8687	3.06	3.06	3.20	0.60	0.08	-3.23	0.08	0.31	-2.89	0.35	98–982
CSD-4	SP-type	1:2.3:2.3	0.6	25	1.7	1.2	530	2181	8.26	8.25	9.31	0.86	0.12	-2.62	0.11	0.38	-2.45	0.41	121–1210
CSD-5	SP-type	1:2.3:2.3	0.5	41	2.0	1.3	924	4267	15.79	15.80	17.15	-0.27	0.08	-1.73	0.05	0.58	-1.78	0.56	183–1833
CSD-6	SP-type	1:2.3:2.3	0.6	6	1.6	1.3	825	14,539	5.77	5.76	5.75	-1.44	0.08	-1.66	0.05	0.60	-1.43	0.70	191–1910

The six samples of this study are from the field photographs. AR, average aspect ratio with I = L I/S, the value of intermediate/short are obtained using CSDCorrections1.50 (Higgins, 2015) and CSDslice 5.0 (Morgan and Jerram, 2006). L/I, the value of long/intermediate was estimated in the field. AF, alignment factor. Number, number of crystals analyzed. Roundness, average roundness of crystals analyzed. Area, area of photo analyzed. Vol phase, volume of plagioclase phenocrysts determined from the area of plagioclase in photo. CSD volume, slope, regression volume, characteristic length (CL), largest intersection is calculated by using CSDCorrections 1.50 (Higgins, 2015). LS slope and LS CL are calculated using least-squares fit and Monte Carlo method (Cheng et al., 2014). Crystallization time = characteristic length (CL)/growth rate (G) (Marsh, 1988, G = 10^{-10}–10^{-9} mm/s).

The logarithm (ln) of population density, the correction factors and the uncertainties for each samples are calculated by using the CSDCorrections 1.50 (Higgins, 2015). The CSD data is embodied in the crystal population density (logarithmic) versus crystal size (long axes) diagram, which can be expressed in three theoretical models including semi-logarithmic distribution (S-CSD), logarithmic distribution (L-CSD) and dispersive distribution (F-CSD).

4. Results

4.1. Plagioclase composition

Anorthite (An) content of all plagioclases with different sizes ranges from An_{18} to An_{54} (mean of An_{31}; Table 2), consistent with a common andesine series. As mentioned above, secondary alteration increases with grain sizes (see the cartoons in Fig. 6). Plagioclase crystals in the matrix are fine grained (0.2–2.3 mm) and subhedral with broader fresh rims, which usually exhibit polysynthetic twins (Fig. 4c, d). Their An contents are variable from 20 to 54. No positive correlation between An content and grain size was observed for plagioclase in the matrix. However, the An contents of the cores are generally higher than those of the rim for a given crystal (Fig. 6). In contrast to the matrix, the plagioclase phenocrysts show strong alteration with large sericitized cores and thin fresh rims (Fig. 4a, 6). Therefore, no reliable data was obtained for the cores of phenocrysts. The grain size of plagioclase phenocrysts increases from the SP-type (3–6 mm), through the central grains of FG-type (4–13 mm) to outer grains of FG-type (10–20 mm, Fig. 6). Chemical compositions of the plagioclase in the SP-type and the outer grains of FG-type are similar, both with slightly higher An contents (An_{35-45}) than the plagioclase matrix (An_{25-35}). The lowest An content (An_{19-22}) was recorded in the plagioclase phenocrysts near the center of the of the FG-type glomerocrysts.

X-ray compositional mapping of the plagioclase glomerocrysts show weak zonations in Na and K for individual crystals (Fig. 7). The core is generally richer in K and poorer in Na relative to the rim (Fig. 7a, b). This feature is more pronounced for the sub-parallel glomerocrysts (Fig. 7c), where the plagioclase rims show wider zonations in Na.

4.2. Garnet composition

To constrain the post-magmatic geological processes, a total of 6 garnet inclusions in the plagioclase phenocrysts have been selected and analyzed by EMPA. All analyzed garnets have high FeO^{Total} (25.26–28.89%), CaO (9.15–10.61%) and low MnO (3.5–7.07%) and MgO (0.21–1.01%) contents. They are mainly composed of a solid solution of almandine-grossular, which constitutes 83% to 89% of the total molecular composition. They have the chemical formula of Alm_{53-63} Gro_{26-30} Sps_{8-16} Prp_{1-5} Adr_{0-2} (Table 3).

4.3. CSD data

We obtained three CSD samples for the flower-like glomerocrysts (FG-type) and six CSD samples for the single isolated phenocrysts (SP-type). Plagioclase in all samples is strongly tabular with similar I/S ratios (1.6 to 2.7; Fig. 8a) and L/I values of almost 1 (Table 1). A calculated CSD aspect ratio of S:I:L = 1:2.3:2.3 is used for all samples for easily comparison. Higgins (2000) has noticed that the variation of the I/L ratio will effect the size scale of the CSD, but different I/S ratios only change the tailing corrections. The modeling of Higgins (1994) is used to estimated the three-dimension shape of plagioclase crystals in the FG- and SP-type samples. Our results show that the phenocrysts are basically tabular and are similar to the Kameni megacrysts (Fig. 8b; Higgins, 1996).

All FG-type samples have curved but non-overlapping CSDs on a classic CSD diagram (L-CSD; Higgins, 2006; Marsh, 1988) (Fig. 9a). They show a concave-up CSD in the size of 0.3–1 cm, followed by a concave-down CSD in the size of 1–6 cm (Fig. 9a). Samples CSD-1-1 and

Table 2
Representative micro-probe analyses of plagioclase matrix and phenocrysts in the Wulong diorite porphyry dykes (content-wt%, size-long axes/mm).

Type	Matrix						SP-type			Outer of FG-type			Center of FG-type		
Fsp. no.	LY01		LY05		LY11		LY18	LY19	LY21	LY14	LY16	LY17	LY26	LY27	LY29
	core	rim	core	rim	core	rim	rim	rim	rim	rim	rim	rim	rim	rim	rim
Size	0.3	0.3	0.5	0.5	2.3	2.3	4.5	4.0	4.2	20	20	19	6	5	5
SiO_2	58.3	61.6	57.9	63.1	57.1	61.9	58.9	55.2	58.9	58.8	58.1	58.9	62.8	63.5	62.6
Al_2O_3	26.2	23.8	26	23.6	27	23.6	25.5	28.1	25.7	25.9	26.4	26.2	23.3	22.7	24.5
SrO	0.4	0.4	0.3	0.3	0.4	0.4	0.4	0.3	0.4	0.4	0.4	0.4	0.4	0.4	0.4
CaO	8.4	5.9	8.4	5.4	9.2	5.6	7.7	9.6	7.7	7.7	8.2	8.2	4.6	3.9	3.8
Na_2O	6.1	8.5	7.1	8.4	6.6	8.6	7.6	5.9	7.4	7.6	7.4	7.4	9.4	9.8	8.3
K_2O	0.1	0.1	0.1	0.1	0.0	0.2	0.1	0.7	0.0	0.1	0.1	0.0	0.0	0.1	1.3
Total	99.5	100.1	99.7	100.8	100.4	100.3	100.2	99.8	100.1	100.5	100.6	101.1	100.5	100.4	100.9
Formulate based on 8 oxygen atoms															
Si	2.6	2.7	2.6	2.8	2.6	2.8	2.6	2.5	2.6	2.6	2.6	2.6	2.8	2.8	2.9
Al	1.4	1.2	1.4	1.2	1.4	1.2	1.4	1.5	1.4	1.4	1.4	1.4	1.2	1.2	1.3
Sr	–	–	–	–	–	–	–	–	–	–	–	–	–	–	–
Ca	0.4	0.3	0.4	0.3	0.4	0.3	0.4	0.5	0.4	0.4	0.4	0.4	0.2	0.2	0.2
Na	0.5	0.7	0.6	0.7	0.6	0.7	0.7	0.5	0.6	0.7	0.6	0.6	0.8	0.8	0.7
K	0.1	–	–	–	–	–	–	0.04	–	–	–	–	–	–	0.07
X_{An}	41	28	39	26	44	26	36	46	36	36	38	38	21	18	19
X_{Ab}	53	72	60	74	56	73	64	50	63	64	62	62	79	82	74
X_{Or}	6	0	1	0	0	1	0	4	1	0	0	0	0	0	7

CSD-2-1 have a similar amount of glomerocryst (20.2–22.5%), while sample CSD-3-1 has less glomerocryst (4.6%). The mean size of the largest intersection for the FG-type samples is 4.5 cm. SP-type samples show a concave-up CSD in the size of 0.3–1 cm, but have almost straight CSDs in the size of 1–6 cm (S-CSD; Fig. 9b). The largest intersection of SP-type samples can be measured is 4.3 cm. The CSD slopes of FG-type samples are higher than SP-type, with the upper regression line fitted by using a least-square fit (Fig. 9c).

The characteristic length (CL = −1/slope) can intuitively reflect the distributions of CSDs compared to the slopes. Our results show that FG-type samples have a larger CL (0.71 to 0.88 cm) than the SP-type (0.31 to 0.60 cm) (Table 1; Fig. 9d). A weak positive correlation is demonstrated between the plagioclase phenocryst content and the characteristic length (Fig. 9d). There is a good consistency between the CL calculated using the CSDCorrections 1.50 and the CL calculated using the least-squares fit (Table 1). However, the CL of sample CSD-1-2 determined by the least-squares fit are larger than sample CSD-2-1,

which is not consistent with the actual field observations. Therefore, the characteristic length calculated by CSDCorrections have been used for this study.

5. Discussion

5.1. Growth history of the plagioclase phenocrysts

With a constant growth rate, the mineral crystal size is generally positively correlated with their nucleation timescale (Higgins, 2006; Marsh, 1988). The characteristic lengths of the FG-type plagioclase phenocrysts are higher than those of the SP-type with values varying from 0.70 to 0.87 cm and from 0.31 to 0.60 cm, respectively (Fig. 9d). The FG-type samples also have a much larger range of plagioclase phenocryst contents than the SP-type (Fig. 9d). As well, a weak positive correlation trend between the characteristic length and the plagioclase phenocryst
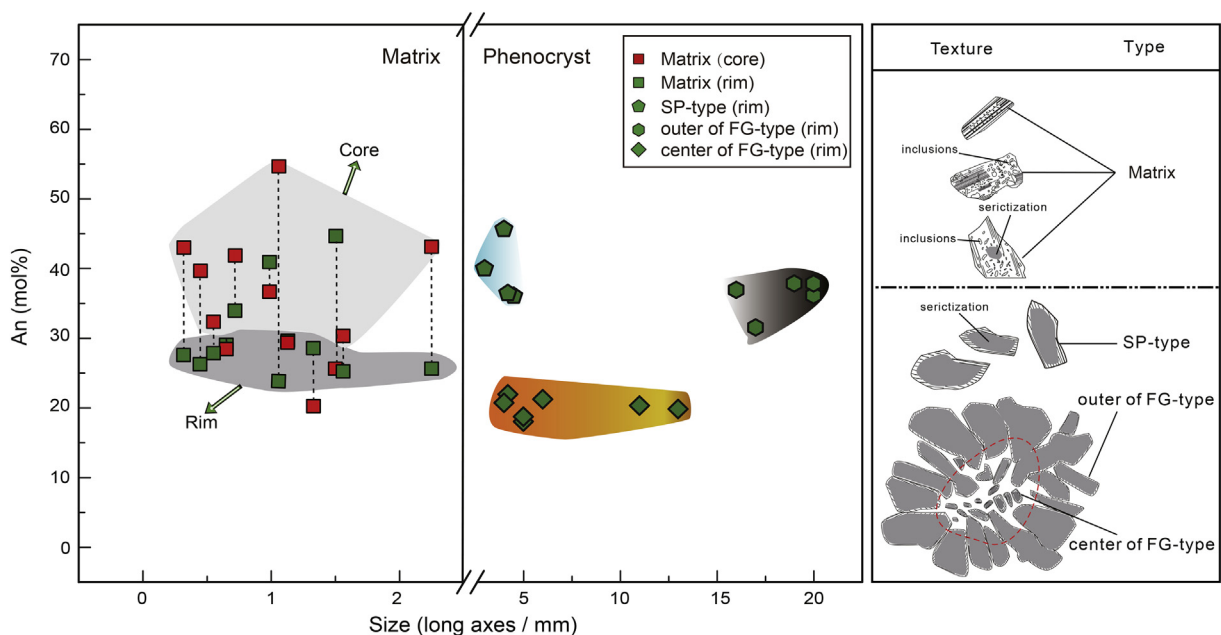
Fig. 6. Plot of Anorthite contents (mol %) versus grain size (long axes/mm) of plagioclase phenocryst and matrix, showing that variable composition of different types of plagioclase.
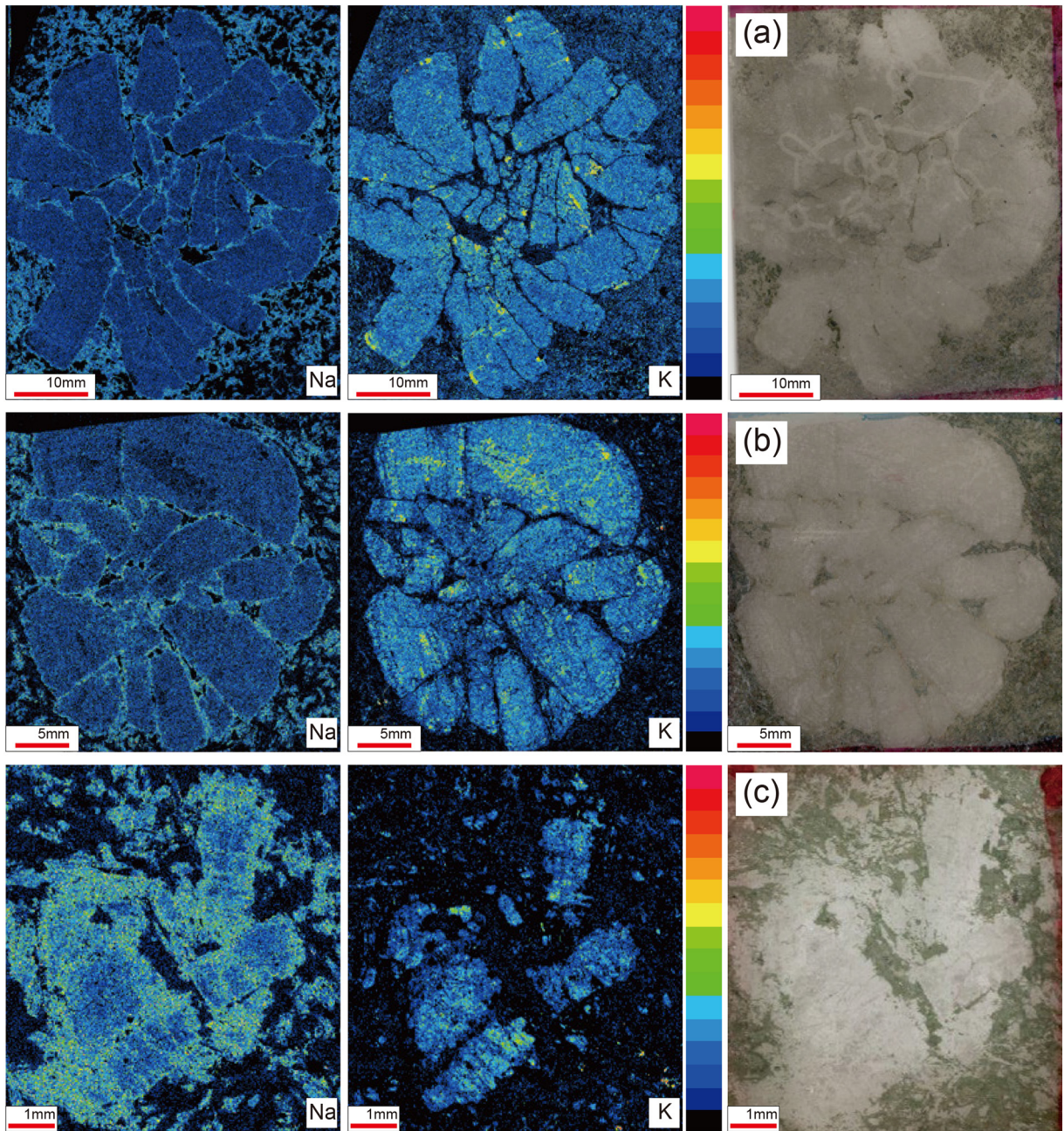
Fig. 7. X-ray compositional maps (Na and K) of the plagioclase glomerocrysts. (a, b) Typical 'flower-like' glomerocrysts. (c) Subparallel synneusis. Elemental abundances increase from cold to warm color in the legend. The third column (on the right) are high-resolution scanned images of thin sections.

content (Fig. 9d). These observations suggest that the FG-type pheno-crysts likely nucleated earlier than the SP-type.

For minerals crystallized in a steady-state system, their ln (popula-tion density) versus crystal size data commonly plot along a straight line (Marsh, 1988), as documented in Fig. 9 (S-CSD). In contrast, if min-eral crystallization is mainly driven by textural coarsening and/or partly affected by fractional crystallization (e.g., Cheng et al., 2014), their ln (population density) versus crystal size data commonly show a con-cave-down CSD with a dramatic decrease in the population density for small crystals (L-CSD in Fig. 9a; Higgins, 1996, 2006, 2011b; Marsh, 1988). In comparison, the concave-up CSD (noted as F-CSD) in Fig. 9a, reflects an adjustment process between crystal size reduction and coarsening balance, which might be controlled by deformation, magma mixing (or mingling) and rejuvenation (kinetic growth) after coarsening (Armienti and Tarquini, 2002; Higgins, 2006; Turcotte, 1997). In our case, the concave-down CSDs in the FG-type samples

with crystal size of 0.5 to 6 cm (Fig. 9a) suggests that they might un-dergo a coarsening process (Cheng et al., 2014; Higgins, 2006, 2011b; Marsh, 1988). The CSDs of the SP-type samples show a steeper slope at the smaller crystals and the larger crystals than the intermediate crys-tals, reflecting a simultaneous process of aggregation, separation and dispersion (Fig. 9b; Higgins, 2006; Marsh, 1988).

Smaller crystals have higher surface areas per unit volume than larger crystals, inducing an excess surface energy. This energy can be dissipated by textural coarsening, in which crystals smaller than a criti-cal size will dissolve and feed the growth of larger crystals simulta-neously (Higgins, 2011b). The lack of small crystals in FG-type plagioclase glomerocrysts further support the existence of coarsening process. Removal of small crystals by coarsening in a crystal mush will enhance the permeability, resulting in focused fluid flows and promot-ing growth and transport of large crystals (Higgins, 1998), which might be responsible for the huge flower-like glomerocrysts.

Table 3
Representative micro-probe analyses of garnet inclusions in the plagioclase phenocryst from the Wulong diorite porphyry dykes (content-wt%).

Sample no.	LY01	LY02	LY03	LY04	LY05	LY06
SiO$_2$	37.45	36.93	37.42	37.88	37.85	37.5
TiO$_2$	0.05	0	0.02	0	0.05	0.44
Al$_2$O$_3$	20.64	20.54	20.94	20.79	20.56	20.22
FeO	24.82	28.89	25.97	25.26	24.74	23.67
MnO	5.25	3.5	4.56	4.89	5.13	7.07
MgO	0.95	0.7	0.81	0.98	1.01	0.21
CaO	10.48	9.15	10.22	10.61	10.25	9.35
Total	99.64	99.71	99.94	100.41	99.59	98.46
Formulate based on 12 oxygens atoms						
Si	3.00	2.99	2.98	3.00	3.01	3.04
Al	1.95	1.90	1.95	1.98	1.95	1.95
Ti	0.00	0.03	0.00	0.00	0.00	0.00
Fe^{3+}	0.04	0.00	0.00	0.00	0.00	0.00
Fe^{2+}	1.62	1.58	1.95	1.74	1.68	1.66
Mn	0.36	0.48	0.24	0.31	0.33	0.35
Mg	0.11	0.02	0.08	0.10	0.12	0.12
Ca	0.90	0.80	0.79	0.88	0.90	0.88
Sum	7.99	7.79	7.98	7.99	7.99	8.00
Almandine	54	53	63	58	55	54
Pyrope	4	1	3	2	4	5
Spessartine	12	16	8	10	12	12
Andradite	2	0	0	0	0	0
Grossular	28	30	26	29	29	29

Almandine-*Alm*, Andradite-*Adr*, Grossular-*Gro*, Pyrope-*Prp*, Spessartine-*Sps*.

Fig. 8. (a) Frequency plot (normalized to 10 to permit comparison) for the width/length of six representative samples. (b) Plot of shape S/I vs. I/L ratios. The square point and bars shows the Kameni megacrysts and Sept Iles massive crystals according to Higgins (1996).

Textural coarsening may occur when crystallization temperature lower or close to the liquids temperature for a long period (e.g. Higgins, 2011b; Simakin and Bindeman, 2008; Yang, 2012; Yang et al., 2014). The variation of magma temperature could be caused by complex convective overturns and/or continuous injections of hot magma (e.g., Cheng et al., 2014; Higgins, 2011a, 2011b; Simakin and Bindeman, 2008). Hence, the coarsening process of our FG-type samples (Fig. 9a) might indicate a continuous injection of pulsating magma in the magma chamber. The FG-type samples show a concave-up CSD from 0.3 to 1 cm (Fig. 9a), suggesting a rejuvenation kinetic process after coarsening, due to injection of new magma (Higgins, 2006; Higgins and Chandrasekharam, 2007).

Interaction between intercept, slope, and crystallinity could reflect magma cooling regime (i.e. cooling rate and system age) within magma chamber (Cashman, 1993). The FG-type samples show similar slopes but different intercepts among samples in the ln vs. crystal size diagram, whereas the SP-type samples are relatively random for both parameters (Fig. 9c). The combined CSDs of both FG-type and SP-type plagioclase phenocrysts in our case are roughly similar to the typical CSD fans (Fig. 9c) (Higgins, 2002; Zieg and Marsh, 2002). Different CSDs may correspond to different cooling regimes (Zieg and Marsh, 2002). The CSDs of FG-type phenocrysts plot on the upper part of the fanning CSDs, indicating a slow solidification rate which results in larger characteristics lengths (Fig. 9d), whereas SP-type phenocrysts may cooled at a faster rate.

The CSDs data have proven to be useful in providing information of crystallization timescale based on the quantitative relationship: crystallization time = characteristic length/growth rate (Cashman, 1993; Higgins, 1996; Marsh, 1988). Accordingly, the accuracy of estimated timescale is highly dependent on the measured characteristic length and the assumed growth rate. The growth rates of plagioclase in sub-volcanic or deeper magma chambers have been documented consistently between 10^{-10} and 10^{-9} mm/s (e.g., Cashman, 1993; Cheng et al., 2014; Higgins and Chandrasekharam, 2007). Assuming a similar growth rate, we calculated the crystallization timescale of the two types of plagioclase phenocryst in the Wulong diorite porphyry dyke using the measured characteristic lengths. The results reveal that the crystallization times of FG-type samples are 278–2782 years, 244–2439 years and 226–2265 years, respectively (mean of 250–2495 years) and the SP type samples are 180–1802 years, 162–1618 years, 98–982 years, 121–1210 years, 183–1833 years and 191–1910 years, respectively (mean of 156–1559 years; Table 1). Although the occurrence of coarsening may lead to the overestimation of residence time calculated by the CSD slope, the calculation of crystallization timescale using average length of both FG- and SP-type samples reveal a similar result with 422–5297 years and 219–4022 years, respectively. This feature indicates that the FG-type plagioclase phenocrysts underwent a longer growth history than the SP-type (Fig. 9d).

5.2. Formation of the flower-like glomerophyric texture

A glomerophyric texture generally forms by plagioclase phenocrysts in volcanic or sub-volcanic rocks. Different models have been proposed to interpret their origins, including: (1) Synneusis model, in which glomerocrysts are irregular and universally zoned, and characterized by massive small crystals attached to the edge of a single large crystal (Hogan, 1985; Kuo and Kirkpatrick, 1982; Schwindinger, 1999; Vance, 1969). (2) Accumulation model, in which laminated crystals accumulate parallel to each other and are asymmetrically zoned (Higgins, 2005; Higgins and Chandrasekharam, 2007; Samuel et al., 2007; Scoates, 2000; Xu et al., 2009). (3) Heterogeneous nucleation model, in which glomerocrysts are irregular or radial, and show an isotropic texture with a random orientation (Cheng et al., 2014; Ikeda et al., 2002; McBirney and Noyes, 1979). (4) Resorption model, where
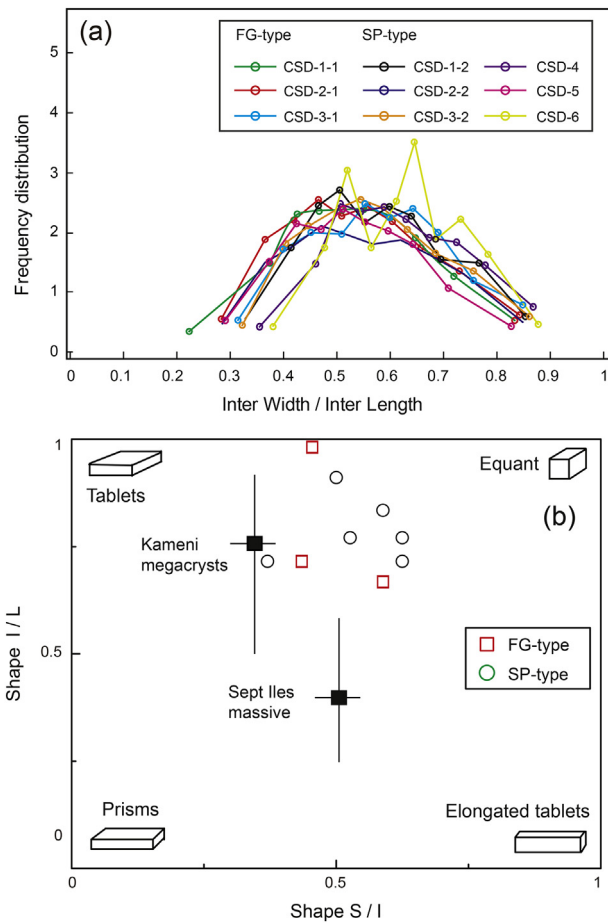
Fig. 9. (a, b) Crystal size distributions of FG-type samples and SP-type samples. The CSDs of FG-type samples are concave, while SP-type samples are nearly straight lines. (c) Linear fitting of CSDs by least square, R is the correlation coefficient. (d) Plot of plagioclase phenocryst content (mol %) versus characteristic length (CL/cm) and crystallization time (year), FG-type has a higher characteristic length and longer growth history than SP-type. The S-CSD, L-CSD and F-CSD are modified after Higgins (2006). The calculated CSDs are modified after Zieg and Marsh (2002).

glomerocrysts are embayed or irregular, and usually exhibit a euhedral overgrowth (Hogan, 1993).

Synneusis model generally results in attachment of plentiful small crystals onto single phenocryst (Kuo and Kirkpatrick, 1982). Accumulation model produces subparallel cumulate crystals at the bottom or the top of a magma chamber driven by gravity flotation (Higgins, 2005; Higgins and Chandrasekharam, 2007; Samuel et al., 2007; Scoates, 2000). Resorption model is caused by changing of intensive parameters, resulting in numerous crystals aggregates along the resorbed margins (e.g. P, T, aH_2O) (Hogan, 1993), which is inconsistent with our observation. The FG-type plagioclase glomerocrysts shows an asymmetrical distribution of concentric plagioclase crystals and relatively tangent grain boundaries (Fig. 2a, b), resembling a broken plagioclase megacryst which had undergone intensive fracturing and collapsing. However, our X-ray composition mapping of both the flower-like and subparallel glomerocrysts show similar compositional zoning in individual plagioclase crystals but not for the whole glomerocryst (Fig. 7). This precludes the fragmentation model and further suggests the flower-like plagioclase glomerocrysts were formed by aggregation and growth of a mass of plagioclase crystals.

The flower-like appearance of plagioclase glomerocryst in our study is somewhat similar to the 'daisy-stone' on the north shore of Lake Superior, which is characterized by a distinctive radiating calcic-plagioclase in a fine grained to aphanitic basaltic matrix (Annells, 1973; Giblin, 1974). It has been considered to result from clustering of large spherulitic crystals under extremely low undercooling degree (Annells, 1973; Giblin, 1974). Similarity, it is possible that the flower-like glomerocryst results from heterogeneous nucleation model, in which different crystals grow radially along different directions (e.g.,

Cheng et al., 2014; Ikeda et al., 2002; McBirney and Noyes, 1979; Špillar and Dolejš, 2015).

Hereby we propose a model in which the formation history of the flower-like glomerophyric texture were divided into five steps (see illustrations Figs. 10, 11). (1) Nucleation and initial growth of crystals start in a confined environment (Fig. 10a), which could be localized swellings in the conduits rather than a large magma chamber (Fig. 11a; Higgins and Chandrasekharam, 2007). (2) Subsequent upwelling of magma carrying early crystals ascend to a shallow magma chamber (Fig. 11b). With lower density, plagioclase crystals will float and adhere together. Sub-parallel glomerocrysts (synneusis) are subsequently formed due to convective movement of magma in the chamber (Fig. 10b; Renjith, 2014; Schwindinger, 1999; Vance, 1969). It is highly possible that plagioclase crystals tend to waft up to the roof and aggregate there during vigorous convection driven by continues injection of hot pulsed magma (Fig. 10c). Mineral resorption process might occur at this stage due to superheating, which might result in partial or complete dissolution of early crystals (Fig. 2f). However, the crystals that survived during dissolution process will continue to coarsen when magma temperature is close to the saturation temperature of plagioclase. Since the roof layer of the magma chamber has a lower undercooling degree, radial coarsening growth on early-nucleated smaller plagioclase crystals or crystals aggregate might dominate the process and finally form a flower-like glomerophyric texture of the plagioclase phenocrysts (Figs. 10d, 11b; Ikeda et al., 2002; McBirney and Noyes, 1979; Špillar and Dolejš, 2015). Low alignment factor (AF) values (5–41; Table 1) of all samples further suggest an radial symmetric growth of the crystals at magma chamber (Higgins, 2006). At different layers of the magma chamber, diversity morphologies of plagioclase glomerocrysts could
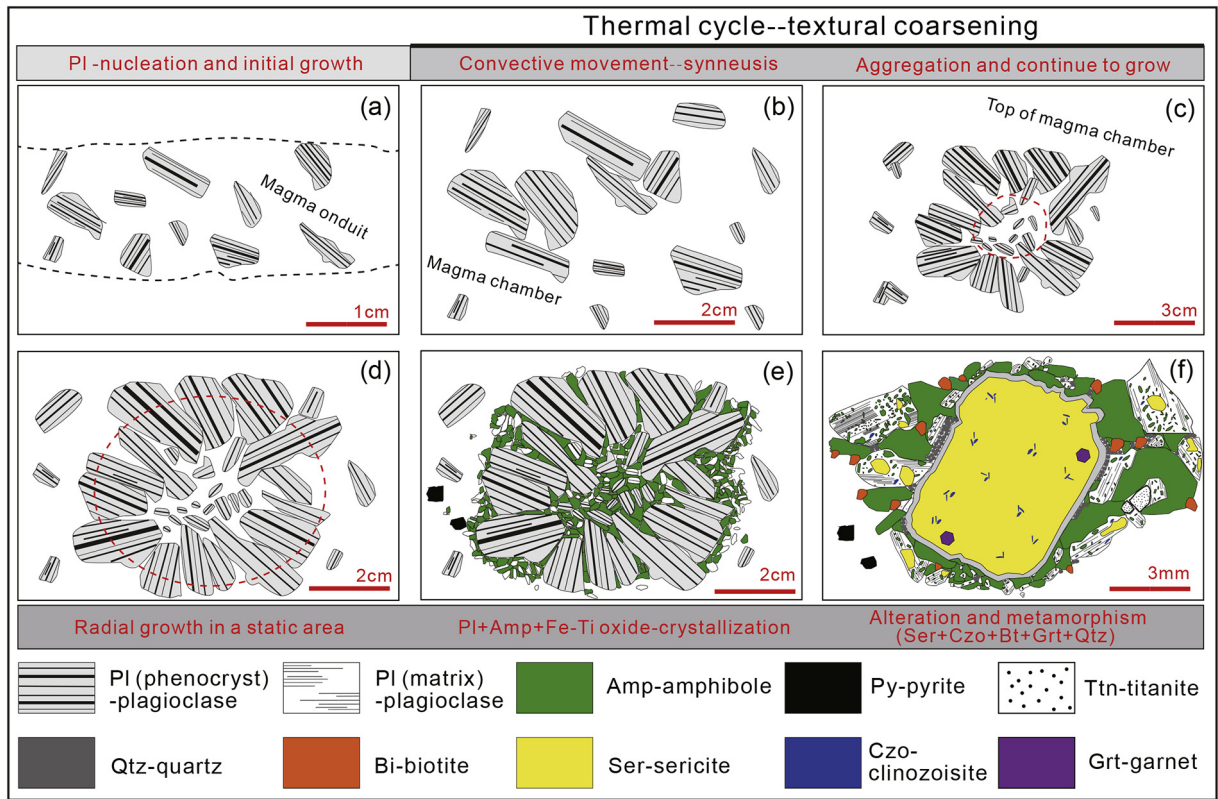
Fig. 10. Schematic cartoon showing the formation processes of the flower-like glomerophyric texture and the crystallization sequence: (a) phenocryst nucleation and initial growth, (b) phenocryst rotation and aggregation, (c) phenocryst aggregation and continue to grow, (d) phenocrysts radial growth, (e) matrix crystalline and (f) late-stage alteration or metamorphism.
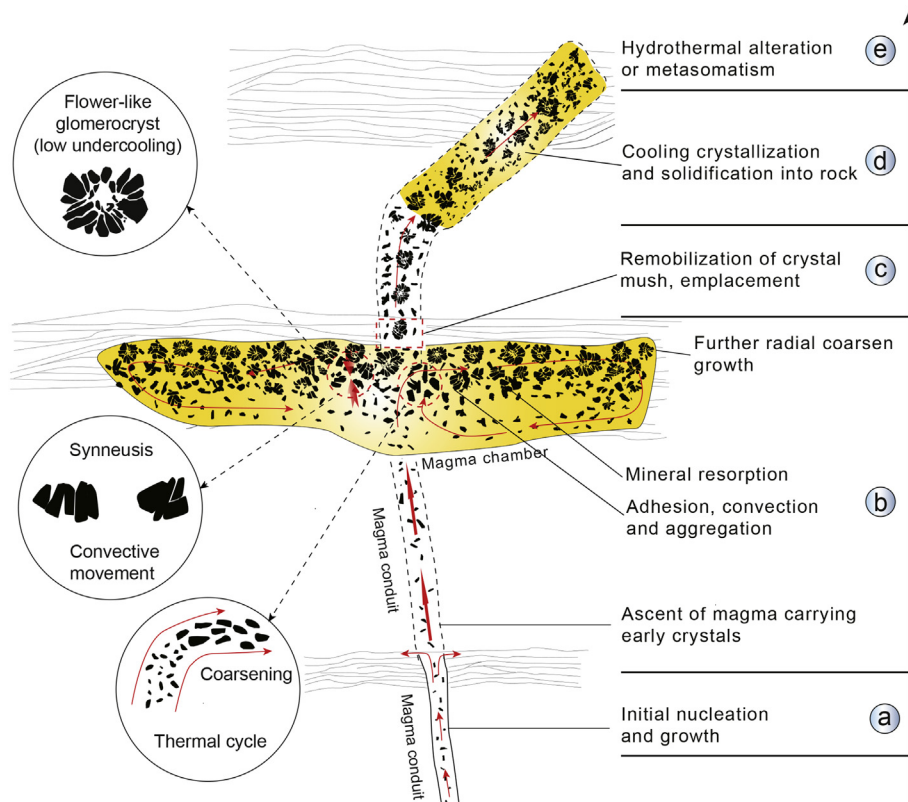
Fig. 11. A genetic model of the magma environment, processes and driven mechanisms during formation of the flower-like glomerophyric diorite porphyry dykes in Wulong.

form due to the variable undercooling degrees which have close relationship with the isotherms (Zieg and Marsh, 2002). (3) Continues injection of hot pulsed magma extends the volume of magma chamber and remobilizes earlier-formed dense crystal mush to rise up along fracture channels to emplace as intrusive dykes (Fig. 11c). The flower-like and other shaped plagioclase glomerocrysts formed in the magma chamber will be taken into shallow levels in response to magma influx. The magmatic flow structure with orientated flower-like plagioclase phenocrysts observed in the outcrop (Fig. 3b), supports that the flower-like plagioclase glomerocrysts can migrate independently as long as they float in sufficient fluids during magma flow (Vernon, 2000; Vernon and Paterson, 2008; Žák et al., 2007). (4) Subsequent after emplacement, rapid magma cooling results in extensive nucleation and crystallization of abundant plagioclase, amphibole, biotite and Fe—Ti oxides which formed the rock matrix (Fig. 10e). Together with the plagioclase glomerocrysts, a diorite porphyry with unusual flower-like glomerophyric structure was finally formed (Fig. 11d). (5) At post-magmatic stage, hydrothermal alteration modified the plagioclase phenocryst from center to rim to form secondary minerals of clinozoisite and sericite (Figs. 10f, 11e). As well on the margin of plagioclase phenocrysts produced euhedral almandine (Table 3) and interstitial quartz due to post-magmatic metamorphism (Fig. 10f).

6. Conclusions

The Wulong diorite porphyry has a typical glomerophyric texture but unusual with flower-like shape. The plagioclase phenocrysts have been divided into FG-type and SP-type based on mineral topography. The FG- and SP-type plagioclases are chemically similar in anorthite contents (An_{35-45}) which are slightly higher than the plagioclase matrix (An_{25-35}). Quantitative texture studies provide information on the duration of crystallization, and indicate that FG-type plagioclase survive and obviously coarsening during the continuous supply of hot magma system. The FG-type plagioclases might have grown in the roof layer of magma chamber with a relatively static condition and a lower undercooling degree. Formation of the flower-like glomerophyric texture underwent two important steps: (1) initial nucleation and growth in a confined environment and (2) ascent with magmas up to magma chamber and further radial coarsen therein.

Acknowledgments

References

Annells, R.N., 1973. Proterozoic Flood Basalts of Eastern Lake Superior: The Keweenawan Volcanic Rocks of the Mamainse Point Area, Ontario. Geological Survey of Canada Paper 72-10 (51 p.).

Armienti, P., Tarquini, S., 2002. Power law olivine crystal size distributions in lithospheric mantle xenoliths. Lithos 65 (3–4), 273–285.

Armienti, P., Perinelli, C., Putirka, K.D., 2013. A new model to estimate deep-level magma ascent rates, with applications to Mt. Etna (Sicily, Italy). J. Petrol. 54 (4), 795–813.

Barbey, P., Ayalew, D., Yirgu, G., 2005. Insight into the origin of gabbro-dioritic cumulophyric aggregates from silicic ignimbrites: Sr and Ba zoning profiles of plagioclase phenocrysts from Oligocene Ethiopian plateau rhyolites. Contrib. Mineral. Petrol. 149 (2), 233–245.

du Bray, E.A., Harlan, S.S., 1996. The Eocene big timber stock, south-Central Montana: development of extensive compositional variation in an arc-related intrusion by sidewall crystallization and cumulate glomerocryst remixing. Geol. Soc. Am. Bull. 11, 1404–1424.

Cashman, K.V., 1993. Relationship between plagioclase crystallization and cooling rate in basaltic melts. Contrib. Mineral. Petrol. 113 (1), 126–142.

Cashman, K.V., Marsh, B.D., 1988. Crystal size distribution (CSD) in rocks and the kinetics and dynamics of crystallization II: Makaopuhi lava lake. Contrib. Mineral. Petrol. 99 (3), 292–305.

Cheng, L.L., Yang, Z.F., Zeng, L., Wang, Y., Luo, Z.H., 2014. Giant plagioclase growth during storage of basaltic magma in Emeishan large Igneous Province, SW China. Contrib. Mineral. Petrol. 167 (2), 1–20.

Cheng, L.L., Wang, Y., Herrin, J.S., Ren, Z.Y., Yang, Z.F., 2017. Origin of K-feldspar Megacrysts in rhyolites from the Emeishan large Igneous Province, Southwest China. Lithos 294, 397–411.

Diwu, C., Sun, Y., Zhao, Y., Lai, S., 2014. Early Paleoproterozoic (2.45–2.20 Ga) magmatic activity during the period of global magmatic shutdown: implications for the crustal evolution of the southern North China craton. Precambrian Res. 255, 627–640.

Dong, Y., Santosh, M., 2016. Tectonic architecture and multiple orogeny of the Qinling Orogenic Belt, Central China. Gondwana Res. 29 (1), 1–40.

Giblin, P.E., 1974. Middle Keweenawan Rocks of the Batachawana-Mamainse Point Area. Institute of Lake Superior Geology 20th Annual Meeting, Nipigon, Ontario, Program, Abstracts, and Field Guides. vol. 20, pp. 39–67.

Giblin, P.E., Armsburst, G.A., 1969. Batchawana, Ontario Department of Mines (Map 2251, scale 1:63 360).

Graeter, K.A., Beane, R.J., Deering, C.D., Gravley, D., Bachmann, O., 2015. Formation of rhyolite at the Okataina volcanic complex, New Zealand: new insights from analysis of quartz clusters in plutonic lithics. Am. Mineral. 100 (8–9), 1778–1789.

Higgins, M.D., 1994. Determination of crystal morphology and size from bulk measurements on thin sections: numerical modeling. Am. Mineral. 79, 113–119.

Higgins, M.D., 1996. Magma dynamics beneath Kameni volcano, Thera, Greece, as revealed by crystal size and shape measurements. J. Volcanol. Geotherm. Res. 70 (1), 37–48.

Higgins, M.D., 1998. Origin of anorthosite by textural coarsening: quantitative measurements of a natural sequence of textural development. J. Petrol. 39 (7), 1307–1323.

Higgins, M.D., 2000. Measurement of crystal size distributions. Am. Mineral. 85 (9), 1105–1116.

Higgins, M.D., 2002. Closure in crystal size distributions (CSD), verification of CSD calculations, and the significance of CSD fans. Am. Mineral. 87, 171–175.

Higgins, M.D., 2005. A new interpretation of the structure of the sept Iles intrusive suite, Canada. Lithos 83 (3), 199–213.

Higgins, M.D., 2006. Verification of ideal semi-logarithmic, lognormal or fractal crystal size distributions from 2D datasets. J. Volcanol. Geotherm. Res. 154 (1–2), 8–16.

Higgins, M.D., 2009. The Cascadia megathrust earthquake of 1700 may have rejuvenated an isolated basalt volcano in western Canada: age and petrographic evidence. J. Volcanol. Geotherm. Res. 179 (1), 149–156.

Higgins, M.D., 2011a. Quantitative petrological evidence for the origin of K-feldspar phenocrysts in dacites from Taapaca volcano, Chile. Contrib. Mineral. Petrol. 162 (4), 709–723.

Higgins, M.D., 2011b. Textural coarsening in igneous rocks. Int. Geol. Rev. 53 (3–4), 354–376.

Higgins, M.D., 2015. CSD Corrections 1.50, http://www.uqac.ca/mhiggins/csdcorrection. html.

Higgins, M.D., 2017. Quantitative investigation of felsic rock textures using cathodoluminescence images and other techniques. Lithos 277, 259–268.

Higgins, M.D., Chandrasekharam, D., 2007. Nature of sub-volcanic magma chambers, Deccan Province, India: evidence from quantitative textural analysis of plagioclase phenocrysts in the Giant plagioclase basalts. J. Petrol. 48 (5), 885–900.

Hogan, J.P., 1985. Glomerophyric plagioclase in epizonal plutons: synneusis or peritectic reaction relationship. Geol. Soc. Am. Abstr. Programs 17 (CONF-8510489-).

Hogan, J.P., 1993. Monomineralic glomerocrysts: textural evidence for mineral resorption during crystallization of igneous rocks. J. Geol. 101 (4), 531–540.

Holness, M.B., Nielsen, T.F.D., Tegner, C., 2006. Textural maturity of cumulates: a record of chamber filling, liquidus assemblage, cooling rate and large-scale convection in mafic layered intrusions. J. Petrol. 48 (1), 141–157.

Ikeda, S., Toriumi, M., Yoshida, H., Shimizu, I., 2002. Experimental study of the textural development of igneous rocks in the late stage of crystallization: the importance of interfacial energies under non-equilibrium conditions. Contrib. Mineral. Petrol. 142 (4), 397–415.

Kuo, L.C., Kirkpatrick, R.J., 1982. Pre-eruption history of phyric basalts from DSDP legs 45 and 46: evidence from morphology and zoning patterns in plagioclase. Contrib. Mineral. Petrol. 79 (1), 13–27.

Lai, Z., Zhao, G., Han, Z., Liu, B., Bu, X., Leng, C., 2016. Back-arc magma processes in the Okinawa trough: new insights from textural and compositional variations of plagioclase in basalts. Geol. J. 51 (S1), 346–356.

Liu, D., Wilde, S.A., Wan, Y., Wang, S., Valley, J.W., Kita, N., Gao, L., 2009. Combined U–Pb, hafnium and oxygen isotope analysis of zircons from meta-igneous rocks in the southern North China craton reveal multiple events in the late Mesoarchean–early Neoarchean. Chem. Geol. 261 (1), 140–154.

Magee, C., O'Driscoll, B., Chambers, A.D., 2010. Crystallization and textural evolution of a closed-system magma chamber: insights from a crystal size distribution study of the Lilloise layered intrusion, East Greenland. Geol. Mag. 147 (03), 363–379.

Marsh, B.D., 1988. Crystal size distribution (CSD) in rocks and the kinetics and dynamics of crystallization. Contrib. Mineral. Petrol. 99 (3), 277–291.

Marsh, B.D., 1998. On the interpretation of crystal size distributions in magmatic systems. J. Petrol. 39 (4), 553–599.

McBirney, A.R., Noyes, R.M., 1979. Crystallization and layering of the Skaergaard intrusion. J. Petrol. 20 (3), 487–554.

Milovanović, D., Karamata, S., Banješević, M., 2005. Petrology of alkali basalts of Zlot, Timok magmatic complex (eastern Serbia). Tectonophysics 410 (1), 501–509.

Morgan, D.J., Jerram, D.A., 2006. On estimating crystal shape for crystal size distribution analysis. J. Volcanol. Geotherm. Res. 154 (1), 1–7.

Putman, G.W., Alfors, J.T., 1969. Geochemistry and petrology of the Rocky Hill stock, Tulare County, California. Geol. Soc. Am. Spec. Pap. 120, 1–106.

Randolph, A.D., Larson, M.A., 1971. Chapter 7–effects of formation and growth kinetics on particle-size distribution. Theory Part. Process. 111–126.

Renjith, M.L., 2014. Micro-textures in plagioclase from 1994-1995 eruption, Barren Island volcano: evidence of dynamic magma plumbing system in the Andaman subduction zone. Geosci. Front. 5 (1), 113–126.

Samuel, M.D., Moussa, H.E., Azer, M.K., 2007. A-type volcanics in central eastern Sinai, Egypt. J. Asian Earth Sci. 47 (4), 203–226.

Schwindinger, K.R., 1999. Particle dynamics and aggregation of crystals in a magma chamber with application to Kilauea Iki olivines. J. Volcanol. Geotherm. Res. 88 (4), 209–238.

Scoates, J.S., 2000. The plagioclase–magma density paradox re-examined and the crystallization of Proterozoic anorthosites. J. Petrol. 41 (5), 627–649.

Seaman, S.J., 2000. Crystal clusters, feldspar glomerocrysts, and magma envelopes in the Atascosa lookout lava flow, southern Arizona, USA: recorders of magmatic events. J. Petrol. 41 (5), 693–716.

Shane, P., 2015. Contrasting plagioclase textures and geochemistry in response to magma dynamics in an intra-caldera rhyolite system, Okataina volcano. J. Volcanol. Geotherm. Res. 297, 1–10.

Simakin, A.G., Bindeman, I.N., 2008. Evolution of crystal sizes in the series of dissolution and precipitation events in open magma systems. J. Volcanol. Geotherm. Res. 177 (4), 997–1010.

Špillar, V., Dolejš, D., 2015. Heterogeneous nucleation as the predominant mode of crystallization in natural magmas: numerical model and implications for crystal–melt interaction. Contrib. Mineral. Petrol. 169 (1), 4.

Turcotte, D.L., 1997. Fractals and Chaos in Geology and Geophysics. Cambridge university press.

Vance, J.A., 1969. On synneusis. Contrib. Mineral. Petrol. 24 (1), 7–29.

Vernon, R.H., 2000. Review of microstructural evidence of magmatic and solid-state flow. Vis. Geosci. 5 (2), 1–23.

Vernon, R.H., Paterson, S.R., 2008. How late are K-feldspar megacrysts in granites? Lithos 104 (1–4), 327–336.

Wang, L.X., Ma, C.Q., Zhang, C., Zhang, J.Y., Marks, M.A.W., 2014. Genesis of leucogranite by prolonged fractional crystallization: a case study of the Mufushan complex, South China. Lithos 206–207 (1), 147–163.

Wang, L.X., Ma, C.Q., Lai, Z.X., Marks, M.A.W., Zhang, C., Zhong, Y.F., 2015. Early Jurassic mafic dykes from the Xiazhuang ore district (South China): implications for tectonic evolution and uranium metallogenesis. Lithos 239, 71–85.

Weinberg, R.F., Sial, A.N., Pessoa, R.R., 2001. Magma flow within the Tavares pluton, northeastern Brazil: compositional and thermal convection. Geol. Soc. Am. Bull. 113 (4), 508–520.

Williams, E., Boudreau, A.E., Boorman, S., Kruger, F.J., 2006. Textures of orthopyroxenites from the Burgersfort bulge of the eastern Bushveld Complex, Republic of South Africa. Contrib. Mineral. Petrol. 151 (4), 480.

Xu, X.W., Jiang, N., Yang, K., Zhang, B.L., Liang, G.H., Mao, Q., Qin, K.Z., 2009. Accumulated phenocrysts and origin of feldspar porphyry in the Chanho area, western Yunnan, China. Lithos 113 (3), 595–611.

Yang, Z.F., 2012. Combining quantitative textural and geochemical studies to understand the solidification processes of a granite porphyry: Shanggusi, east Qinling, China. J. Petrol. 53 (9), 1807–1835.

Yang, Z.F., Luo, Z.H., Lu, X.X., Huang, F., Chen, B.H., Zhou, J.L., Cheng, L.L., 2014. The role of external fluid in the Shanggusi dynamic granitic magma system, east Qinling, China: quantitative integration of textural and chemical data. Lithos 208, 339–360.

Žák, J., Paterson, S.R., Memeti, V., 2007. Four magmatic fabrics in the Tuolumne batholith, Central Sierra Nevada, California (USA): implications for interpreting fabric patterns in plutons and evolution of magma chambers in the upper crust. Geol. Soc. Am. Bull. 119 (1–2), 184–201.

Zieg, M.J., Marsh, B.D., 2002. Crystal size distributions and scaling laws in the quantification of igneous textures. J. Petrol. 43 (1), 85–101.